Characterization and Engineering Properties of Dry and Ponded Class-F Fly Ash

R. C. Bachus, P.E., M.ASCE[1]; M. Terzariol[2]; C. Pasten[3]; S. H. Chong[4]; S. Dai, A.M.ASCE[5];
M. S. Cha, A.M.ASCE[6]; S. Kim, A.M.ASCE[7]; J. Jang, A.M.ASCE[8]; E. Papadopoulos[9];
S. Roshankhah, A.M.ASCE[10]; L. Lei[11]; A. Garcia[12]; J. Park[13]; A. Sivaram[14];
F. Santamarina[15]; X. Ren[16]; and J. C. Santamarina[17]

Abstract: Characterization studies conducted on Class-F fly-ash specimens gathered from different producers in the southeastern United States confirm general trends reported for fly ash worldwide. Additional tests and detailed analyses explain the spread in specific gravity (interparticle porosity cenospheres), highlight the tendency to segregation and layering, and show marked ferromagnetism. Furthermore, data show that early diagenetic cementation—within days after wetting—hinders densification and produces a fabric that is prone to collapse. New procedures are specifically developed to diagnose and characterize early diagenesis, including (1) pH measurements as an indicator of diagenetic potential, (2) test protocols to assess early diagenesis using oedometer tests and shear-wave velocity, and (3) procedures to determine realizable unit weights as reference values for the analyses of contractive or dilative tendencies and instability. In the absence of early diagenetic cementation, dilative fly-ash behavior is expected in the upper $\approx$20 m under monotonic shear loading. Flow instability may follow the failure of the containment structure if the ponded ash is saturated and has experienced hindered densification. **DOI: [10.1061/(ASCE)GT.1943-5606.0001986](https://doi.org/10.1061/(ASCE)GT.1943-5606.0001986).** *This work is made available under the terms of the Creative Commons Attribution 4.0 International license, http://creativecommons.org/licenses/by/4.0/.*

Introduction

Fly ash is a fine-grained by-product of coal combustion. The United States alone produces over 50 million t per year. Around 45% is reused, and the rest is disposed of in ponds and landfills (ACAA 2014). The failure of the Tennessee Valley Authority's Kingston Fossil Plant containment embankment in 2008 led to the release of 500 million gal. (1.9 million m^3) of ponded fly ash and triggered a national debate regarding the safety of fly-ash storage systems and conditions that result in the static liquefaction and flow of ponded fly ash.

This paper documents a comprehensive study of Class-F fly ash. First, data trends compiled from published reports on fly ash produced around the world are presented. Then, results obtained from several studies conducted on fly ash produced in the southeastern United States are summarized. The paper features new procedures specifically developed to investigate and characterize some unique characteristics of fly ash.

[1]Geosyntec Senior Principal, Geosyntec Consultants, Kennesaw, GA 30144. Email: RBachus@Geosyntec.com

[2]Research Scientist, Dept. of Earth Science and Engineering, King Abdullah Univ. of Science and Technology, Thuwal 23955, Saudi Arabia (corresponding author). ORCID: https://orcid.org/0000-0001-5362-1968. Email: marco.terzariol@kaust.edu.sa

[3]Assistant Professor, Departamento de Ingeniería Civil, Universidad de Chile, Santiago, Santiago de Chile 8370449, Chile. Email: cpasten@ing.uchile.cl

[4]Assistant Professor, Dept. of Civil Engineering, Sunchon National Univ., 255, Jungang-ro, Sunchon-si, Jeollanam-do 57922, Republic of Korea. Email: shchong@scnu.ac.kr

[5]Assistant Professor, School of Civil and Environmental Engineering, Georgia Tech, Atlanta, GA 30332. Email: sheng.dai@ce.gatech.edu

[6]Assistant Professor, Zachry Dept. of Civil Engineering, Texas A&M, College Station, TX 77843. Email: mcha@civil.tamu.edu

[7]Assistant Professor, College of Engineering, Univ. of Nebraska–Lincoln, Lincoln, NE 68588. Email: seunghee.kim@unl.edu

[8]Geoscientist, Dept. of Earth Science and Engineering, King Abdullah Univ. of Science and Technology, Thuwal 23955, Saudi Arabia. Email: junbong.jang8@gmail.com

[9]Formerly, Postdoctoral Researcher, Strategic Decisions Group, Flat 1, 155 King's Rd., London SW3 5TX, UK. Email: epapadop@outlook.com

[10]Postdoctoral Scholar, Dept. of Mechanical and Civil Engineering, Caltech, Pasadena, CA 91125. Email: shroshankhah@gmail.com

[11]Postdoctoral Scholar, National Energy Technology Laboratory, Dept. of Energy, 3610 Collins Ferry Rd., Morgantown, WV 26505. Email: Lei@netl.doe.gov

[12]Ph.D. Candidate, Dept. of Earth Science and Engineering, King Abdullah Univ. of Science and Technology, Thuwal 23955, Saudi Arabia. Email: Adrian.garcia@kaust.edu.sa

[13]Postdoctoral Scholar, Dept. of Earth Science and Engineering, King Abdullah Univ. of Science and Technology, Thuwal 23955, Saudi Arabia. Email: junghee.park@kaust.edu.sa

[14]Geotechnical Engineer, Water Division, Black & Veatch, 5716 Dunham Rd., Downers Grove, IL 60516. Email: aswathy@outlook.com

[15]Ph.D. Candidate, Evans School of Public Policy and Governance, Univ. of Washington, Seattle, WA 98103. Email: fjsantam@uw.edu

[16]Assistant Professor, Dept. of Engineering, China Univ. of Geosciences, Wuhan, Hubei 430074, China. Email: xingweiren@cug.edu.cn

[17]Professor, Dept. of Earth Science and Engineering, King Abdullah Univ. of Science and Technology, Thuwal 23955, Saudi Arabia. Email: carlos.santamarina@kaust.edu.sa

© ASCE   04019003-1   J. Geotech. Geoenviron. Eng.

J. Geotech. Geoenviron. Eng., 2019, 145(3): 04019003

Table 1. Fly-ash properties using data trends compiled from published reports on fly ash produced around the world

Property	Symbol	Reported cases	Unit	Range[a]		Statistics[b]	
				Minimum	Maximum	μ	σ
Chemical composition	SiO_2	47	% by weight	27	64	47.7	11.0
	Al_2O_3		% by weight	7.0	38	23.6	7.5
	Fe_2O_3		% by weight	1.7	33	10.4	7.5
	CaO		% by weight	0.5	27	7.0	7.5
Basicity	pH[c]	9	—	7.2	12.6	9.4	2.1
Grain-size distribution	D_{100}	68	μm	60	1,960	442	464
	D_{60}		μm	8.0	120	32	22.6
	D_{30}		μm	2.5	50	13.6	9.8
	D_{10}		μm	0.4	15	5.0	3.8
	C_u		—	2.1	25	7.8	5.5
	C_c		—	0.6	3.9	1.4	0.8
Specific surface	S_s	18	m^2/g	0.09	1.3	0.45	0.39
Liquid limit	LL	11	%	30	62	44.1	10.4
Specific gravity	G_s	76	—	1.50	3.02	2.27	0.3
Porosity	n	26	—	0.36	0.64	0.50	0.08
Hydraulic conductivity	K[d]	172	cm/s	4×10^{-7}	4×10^{-4}	3.8×10^{-5}	3.3×10^{-4}
Friction angle	ϕ	95	Degrees	26	43	36.7	4.9
Compressibility	C_c[d]	92	—	0.04	0.37	0.11	0.08
	C_v	Range	m^2/s	2.20×10^{-8}	9.50×10^{-5}	N/A	N/A

Sources: Data from Acosta et al. (2003), Aineto et al. (2005, 2006), Amonette et al. (2003), Bin-Shafique et al. (2002), Cheerarot and Jaturapitakkul (2004), Cousens and Stewart (2003), Das and Yudhbir (2006), DiGioia Jr. et al. (1995), Du et al. (2013), Gray and Lin (1972), Kaniraj and Gayathri (2004), Kim and Prezzi (2008), Kim et al. (2005), Mishra and Das (2008), Mishra and Karanam (2006), Palmer et al. (2000), Pandian (2004), Prashanth et al. (2001), Premchitt and Evans (1995), Reyes and Pando (2007), Senol et al. (2003), Siddique et al. (2007), Torrey (1978), Trivedi and Sud (2004), Trivedi and Sud (2007), Tu et al. (2007), and Young (1993).
[a]Between 5th and 95th percentile.
[b]After removing 5% of extreme data points to avoid outliers.
[c]Limited data set has bimodal distribution.
[d]Statistics assume lognormal distribution.

Previous Studies

Fly ash recovered from boilers and ponds exhibits a wide range of characteristics and properties. Table 1 summarizes an extensive database compiled from published studies (fly ash produced in North America, Asia, and Europe). This table supports the following observations regarding the chemical, hydraulic, and mechanical properties of fly ash (data sources are listed in the table):

- Silica SiO_2 is the dominant component, followed by alumina Al_2O_3. Calcium oxide CaO is often present. The pH ranges from 7.2 to 12.6.
- The specific gravity of fly ash varies from $G_s < 2.0$ to $G_s > 2.6$. Typically, fly ash is a well-graded silt (mean $C_u \approx 8$), with a median grain diameter $D_{50} = 30 \pm 20$ μm. Sintered millimeter-size aggregations are common.
- The specific surface varies from 0.09 to 1.3 m^2/g. The liquid limit is in the range of LL = 44 ± 10. Most fly-ash specimens classify as low-plasticity silts ML on the United Soil Classification System Casagrande chart.
- Measured hydraulic conductivity values span three orders of magnitude, from 4×10^{-4} to 4×10^{-7} cm/s, and are consistent with specific surface and liquid limit values.
- The porosity of ponded fly ash and porosity attained in laboratory specimens typically varies between $n = 0.36$ and $n = 0.64$. However, a few studies reported extreme porosities, either very dense $n \approx 0.2$ or very loose $n \approx 0.7$.
- Published values of effective friction angle vary between $\phi = 26°$ and $43°$ (for compacted and in situ samples); in most cases, there is not enough information to discern whether reported values are for peak and constant-volume shear, yet there is evidence that dense specimens—relative densities $D_r \geq 80\%$—exhibit high friction angles, i.e., dilatancy is included.

- Compression tests under zero lateral strain show low compressibility even at high void ratios. The compression index $C_c = 0.04$–0.37 is within the range of low-plasticity fines. The coefficient of consolidation is estimated from published deformation-time data in most cases; values span four orders of magnitude, from $c_v \approx 10^{-8}$ to 10^{-4} m^2/s.

Experimental Study: Procedures and Results

Scope of the Study: Specimens and Tests

This paper summarizes the results of several studies conducted on Class-F fly ash. Samples were collected from ash ponds and hoppers at 38 different coal combustion plants in the southeastern United States. Half of the specimens had never been in contact with water. Altogether, the wide range of tests (Table 2) included (1) general characterization tests (grain-size distribution, plasticity, pH, imbibition, specific gravity, electrical and magnetic properties, and scanning electron microscopy), (2) depositional characteristics (tendency to segregation and layering and realizable densities), (3) hydraulic conductivity, (4) mechanical response (oedometer tests, small-strain stiffness, and both drained and undrained triaxial tests), and (5) tendency to early diagenetic cementation. The following sections review the test procedures and results.

General Characteristics: Index Properties

Particle Shape
Fly ash forms from molten droplets. The chemical composition—iron content—and long exposure to high boiler temperatures determine the general characteristics of fly-ash particles (Fisher et al. 1976).

© ASCE 04019003-2 J. Geotech. Geoenviron. Eng.

J. Geotech. Geoenviron. Eng., 2019, 145(3): 04019003

Table 2. Summary of tests conducted as part of this study on specimens obtained from 38 different coal-burning plants in the southeastern United States

Test category	Test	Number of tests	Typical results
Imaging	SEM	45	Cenospheres (some show gypsum crystals)
	X-ray (Shelby tube)	14	Layered stratigraphy
Index	Specific gravity G_s	32	1.96–2.66
	Liquid limit	9	26%–62%
	Plastic limit	9	22%–55%
	Electrical sensitivity	4	Low electrical sensitivity to pore fluid chemistry
	Grain-size distribution	24	D_{50} = 0.01–0.04 mm; C_u = 2.3–4.2[a]
	pH	31	6–12
New index tests	Realizable unit weight	68	Minimum = 5.5 kN/m³; maximum = 15.1 kN/m³
	Formation effects	9	Segregation and layering developed in all sedimentations tests
	Ferromagnetism	29	Some present in all specimens. Up to 20% by weight
	Contact angle	6	Nonwetting (water)
Advanced tests	Oedometer and diagenesis	9	High-pH specimens are prone to early diagenetic cementation
	Oedometer and shear-wave velocity	17	Undisturbed: $\alpha = 21.8–244$ m/s; $\beta = 0.06–0.36$; Remolded: $\alpha = 12–79$ m/s; $\beta = 0.22–0.37$[b]
	Hydraulic conductivity	15	6.7×10^{-5} to 1.8×10^{-4} cm/s
	Constant-volume shear in AC triaxial[c]	44	CD: $\phi'_{peak} = 31°–38°$; $\phi'_{cv} = 29°–36°$; CU: $\phi'_{max} = 28°–36°$
	Cyclic triaxial	7	Response depends on relative realizable density

Note: CD = consolidated drained; CU = consolidated undrained; and SEM = scanning electron microscope.
[a]Range for a 95% confidence interval in a lognormal distribution.
[b]Parameters defined in Eq. (3).
[c]Specimens from eight different power plants; AC = axial compression test.

Most particles in fly-ash specimens are hollow spherical particles known as cenospheres and plerospheres, i.e., nested cenospheres [Figs. 1(a and b)]. These hollow particles imply gas generation in the presence of a molten mineral; indeed, a molten phase and the concurrent release of CO_2 gas occur between 1,200°C–1,400°C during coal burning (Lin et al. 1994; Song et al. 2011). The formation of plerospheres suggests that gas release continues within an existing molten bubble (Fenelonov et al. 2010; Fisher and Natusch 1979).

Not all fly-ash particles are individual closed shells. There are some perforated or burst frozen bubbles that contribute intraparticle porosity [Fig. 1(c)] and millimeter-size conglomerates that form when ash grains sinter together. Finally, some specimens consist of gypsum crystals [Fig. 1(d)].

Grain-Size Distribution
A combination of sieve analysis and hydrometer tests were used to determine the complete grain-size distribution of the tested specimens according to ASTM D421 (ASTM 2007a) and ASTM D422 (ASTM 2007b). Fig. 2 illustrates grain-size distribution data gathered in this study in comparison with the envelope of published data (Table 1). Most particle diameters ranged from $D_{10} = 10$ μm to $D_{90} = 40$ μm, and the coefficient of uniformity is $C_u = 4–20$. All tested fly ash fall under fines-controlled mechanical and hydraulic properties, and are classified as F(F) in the revised soil classification system (RSCS) (Park and Santamarina 2017).

Fines Classification: Atterberg Limits and Electrical Sensitivity
The falling cone procedure was used to determine the liquid limit (LL) according to BS 1377-2 (BS 1990) and the standard rolled-thread method for the plastic limit (PL) using ASTM D4318 (ASTM 2017a). The specimens exhibited low plasticity, typically LL < 62 and plastic index (PI) = LL − PL < 10, and are classified as low-plasticity silts ML on the Casagrande chart [Fig. 3(b)].

Furthermore, liquid limits were determined with kerosene, deionized water, and NaCl brine for four fly-ash specimens to assess the electrical sensitivity to changes in pore fluid chemistry (Jang and Santamarina 2016; Jang and Santamarina 2017). Results plotted in Fig. 3(b) indicate that fly ash can be considered low-plasticity sediments with low electrical sensitivity to pore fluid chemistry; therefore all tested fly-ash specimens are classified as L/L.

Specific Gravity
Specific gravity was measured with water, kerosene, and benzyl alcohol to test the potential effect of wetting fluids on the values of specific surface when the particles have an accessible internal porosity following ASTM C311/C311M (ASTM 2017b) and ASTM C188 (ASTM 2009). Fig. 4 shows no systematic differences between the values measured with different fluids. The inset shows that a water droplet does not experience spontaneous imbibition into the fly-ash specimen.

Most importantly, the measurements $G_s = 1.96–2.66$ confirm the wide range of specific gravities observed in fly ash produced worldwide (histogram superimposed on Fig. 4, and the range is given in Table 1). Although there is a tendency toward lower specific gravity for coarser specimens (Fig. 2), the wide variation in the specific gravity reflects the presence of intraporous cenospheres in all cases (Fig. 1). Therefore, the computation and meaning of standard parameters require careful consideration in fly-ash engineering analyses, including grain size from the hydrometer test, degree of saturation, and void ratio (e.g., for liquefaction).

pH and Spontaneous Imbibition
Simple pH and imbibition tests reflect the interaction between fluids and grains. pH values were obtained using pH strips and fly-ash pastes prepared with deionized water at the liquid limit. Measurements showed pH values that ranged between pH = 6 and 12. Spontaneous imbibition is a measure of particle-level wettability. Water droplets did not readily imbibe dry fly-ash specimens in most cases (inset in Fig. 4). Nonwetting conditions added further difficulty and uncertainty to the determination of the specific gravity, particularly when specimens included intraporous grains with accessible porosity [Fig. 1(d)].
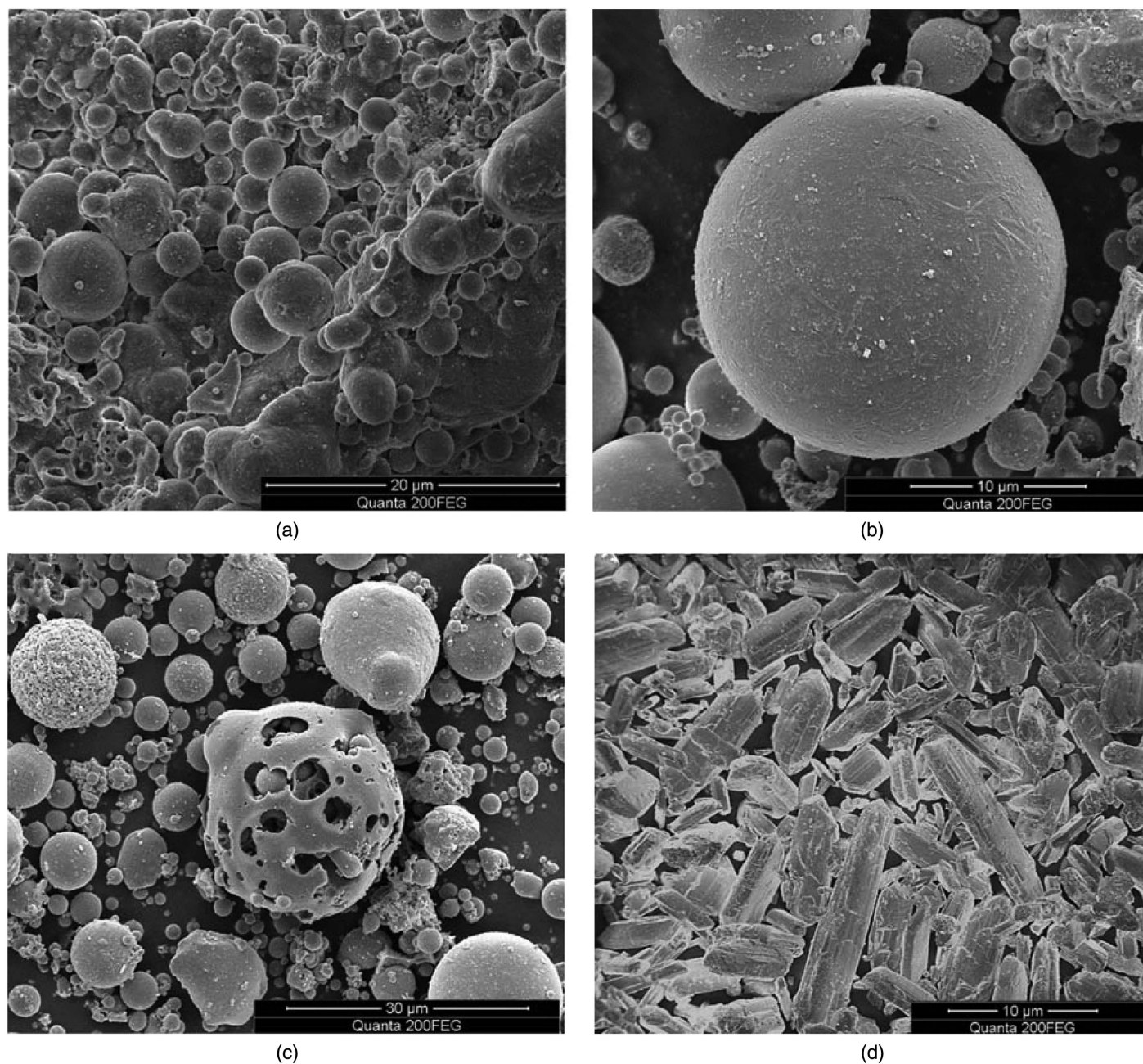
© ASCE   04019003-3   J. Geotech. Geoenviron. Eng.

J. Geotech. Geoenviron. Eng., 2019, 145(3): 04019003

Fig. 1. Scanning electron micrographs: (a and b) spherical fly-ash particles; (c) cenospheres with accessible internal porosity; and (d) gypsum crystals.

Ferromagnetism

The amount of ferromagnetic particles was determined by a process of magnetic separation. The mass fraction of ferromagnetic particles was as high as 20% in some specimens. Therefore the interpretation of electromagnetic measurements and field characterization methods must take into consideration not only the electrical conductivity and dielectric permittivity but the magnetic permeability as well.

Depositional Characteristics

Realizable Unit Weights

The void ratio is not an adequate state parameter for fly ash because of grain intraporosity and the uncertainty in the specific gravity,

as mentioned previously. Thus, it is here recommend using dry unit weights in the analysis of lab and field data, rather than the void ratio.

There are no standards to obtain the maximum and minimum unit weights of fine-grained media such as fly ash. Multiple methods were explored across six orders of magnitude in embodied energy density, including standard Proctor compaction (6×10^5 J/m^3), Harvard minicompaction (4×10^5 J/m^3), tapping compaction (4×10^4 J/m^3), free fall through a funnel in air and in water (3–6×10^2 J/m^3), and formation under shear (dry specimens, 1.5×10^{-1} J/m^3).

The test procedure for formation under shear consists of the following steps: (1) weigh and place 150 g of oven-dried fly ash in a transparent cylinder [internal diameter (ID) = 63 mm and L = 290 mm]; (2) incline and rotate the cylinder gently on a flat surface
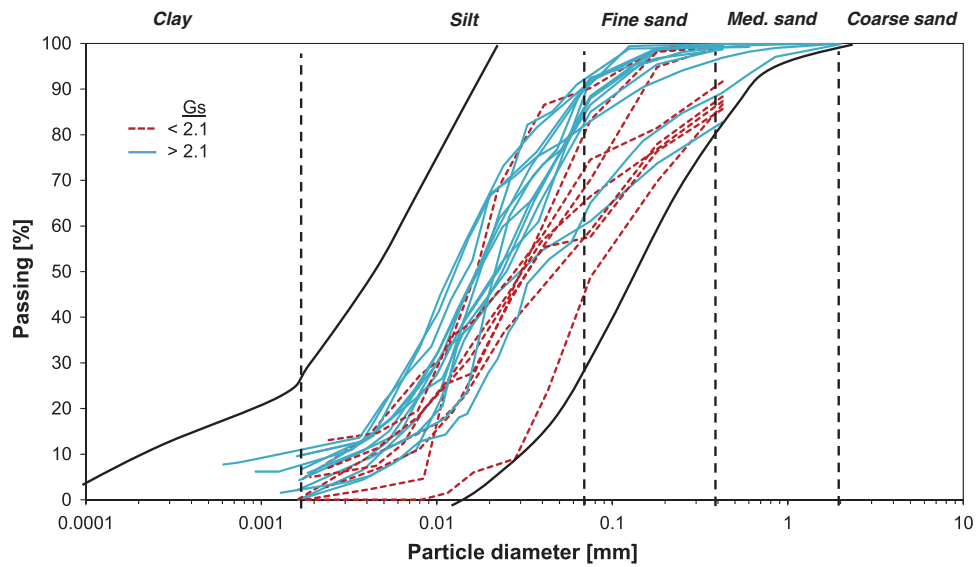
© ASCE 04019003-4 J. Geotech. Geoenviron. Eng.

J. Geotech. Geoenviron. Eng., 2019, 145(3): 04019003

Fig. 2. (Color) Grain-size distribution (24 fly samples). Curves are colored according to specific gravity. Solid black lines bound grain-size distributions compiled from published reports on fly ash produced around the world.
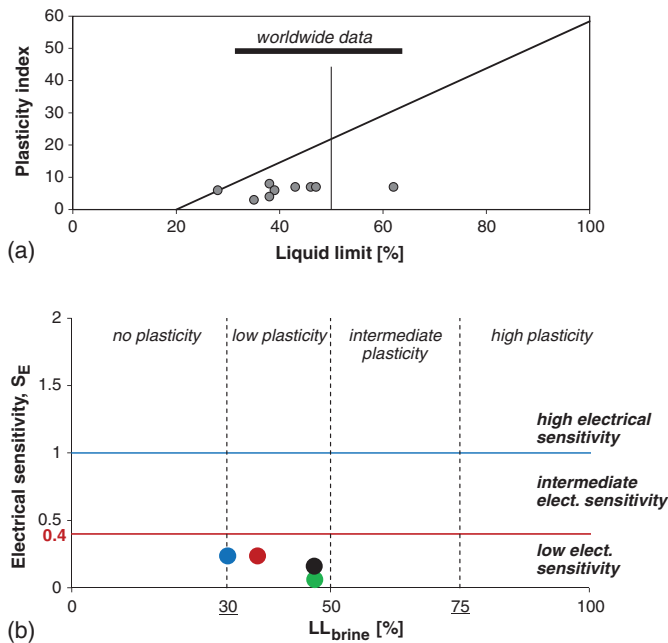

Fig. 3. (Color) Atterberg limits and electrical sensitivity to pore fluids: (a) samples tested in this study plotted on the Casagrande chart, with the range in liquid limit data reported for fly-ash specimens around the world shown as a thick line; and (b) electrical sensitivity chart.
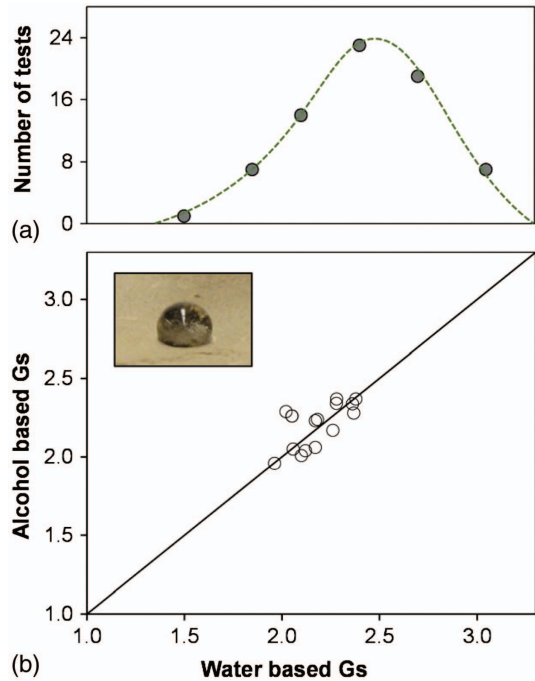
Fig. 4. (Color) Specific gravity: (a) histogram of worldwide data (76 values); and (b) comparison of specific gravity values G_s obtained using water and benzyl alcohol (16 specimens measured using both fluids).

at a rate of one rotation every 10 s; (3) continue the rotation motion, gradually tilting the cylinder back to the upright position; and (4) measure the final sediment height and compute the unit weight.

Proctor compaction and formation under shear consistently produced the maximum and minimum dry unit weights for the 17 fly-ash specimens tested (fly-ash specimens reached the peak dry unit weight in the standard Proctor test at a

compaction water content near the zero-air-voids line). The minimum and maximum realizable dry unit weights measured in this study varied from the lowest $\gamma_{\mathrm{dry,min}} = 5.5 \ \mathrm{kN/m^3}$ to the highest $\gamma_{\mathrm{dry,max}} = 15.1 \ \mathrm{kN/m^3}$.

Fig. 5 illustrates the unit weights obtained with different energy densities. To facilitate the comparison across all samples, the relative density D_r, defined in terms of the unit weight $\gamma_{\mathrm{dry,min}}$ obtained from formation under shear and the unit weight $\gamma_{\mathrm{dry,max}}$ obtained from standard Proctor compaction, was plotted

© ASCE　　　　　　　　　　04019003-5　　　　　　　　　　J. Geotech. Geoenviron. Eng.
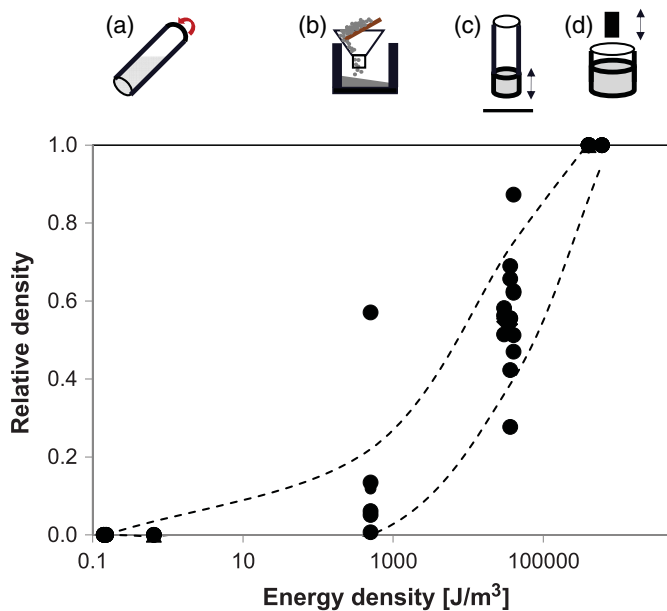
J. Geotech. Geoenviron. Eng., 2019, 145(3): 04019003

Fig. 5. Relative density in terms of realizable unit weights as a function of energy density (68 test results obtained using 17 samples). Specimen formation methods: (a) formation under shear; (b) free fall through a funnel; (c) tapping compaction; and (d) Harvard minicompaction tests.

$$D_r = \frac{\gamma_{\text{dry}} - \gamma_{\text{dry,min}}}{\gamma_{\text{dry,max}} - \gamma_{\text{dry,min}}} \qquad (1)$$

Although trends in unit weights varied widely for all specimens, the relative unit weight D_r data collapse onto a single trend versus energy density for all specimens. Overall, results from this study demonstrate that the selected minimum and maximum dry unit weights are reliable and clearly reflect ash-specific characteristics. Hence, the relative density defined in terms of realizable unit weights is a robust parameter that can be used to compare the experimental results gathered from different fly-ash samples.

Segregation, Layering, and Hydraulic Conductivity
More than 90% of the fly-ash mass reached the bottom of 500-mL graduated cylinders in less than 120 min in all hydrometer tests conducted as part of this study. Additional tests performed in larger transparent tubes highlighted the pronounced tendency to layering during wet deposition (tube dimensions = 700 mm high and 100 mm in diameter; fly-ash slurries prepared at a water content equal to twice the liquid limit, $w = 2 \cdot \text{LL}$; deposition in three stages 30 min apart). Segregation-induced millimeter-scale layering is readily seen in all X-ray images of Shelby tubes recovered from ash ponds throughout this project (see examples in Fig. 6). Therefore, it was concluded that segregation and layering are ubiquitous in water-deposited ash.

These millimeter-scale features have pronounced implications on pond performance, such as marked anisotropy in hydraulic conductivity (preferential horizontal drainage), stiffness, and strength (planar failure surfaces), as well as potential water entrapment in the form of perched layers.

Hydraulic Conductivity
Falling-head permeability tests were run on 15 water pluviated specimens (transparent tube with ID = 100 mm; hydraulic gradients $i \leq 4$). Measured values ranged from 6.7×10^{-5} to
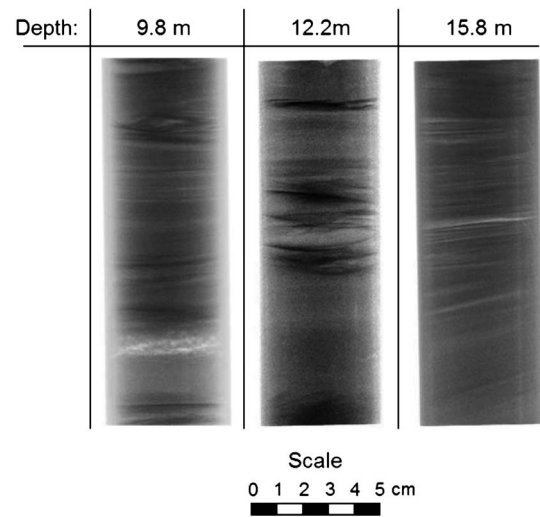

Fig. 6. Segregation and layering in ponds formed by wet deposition. X-ray images of specimens recovered using thin-wall Shelby tubes. These three specimens were recovered from the same borehole at three different depths.

1.8×10^{-4} cm/s. These values agree with those reported in the literature (Table 1). Similar to natural soils, the hydraulic conductivity of fly ash decreases with densification and follows a power function of void ratio e (Kaniraj and Gayathri 2004; Pandian 2004). Void ratio is used here to facilitate the comparison with trends observed for a wide range of soils compiled by Ren and Santamarina (2018)

$$\frac{k}{k_o} = \left(\frac{e}{e_o}\right)^{\delta} \qquad (2)$$

where permeability k_o at nominal void ratio $e_o = 1.0$ is inversely proportional to the square of the specific surface of the fly ash $(S_s)^{-2}$. The exponent δ captures the sensitivity of the permeability to changes in void ratio—primarily interparticle pores—and is $\delta \approx 3\text{–}4$.

Static Compressibility and Stiffness

K_o Compressibility
A standard oedometer cell was used to investigate the static densification of fly ash under zero-lateral-strain conditions. Measured values for the compression index C_c shown in Fig. 7 are within the range of values in the published literature $C_c = 0.11 \pm 0.08$ (Table 1). There is no clear trend between compressibility and dry unit weights.

Small-Strain Stiffness: Shear-Wave Velocity
Bender elements installed in the top and bottom caps allowed concurrent shear-wave measurements to be collected during consolidation tests. The tests were conducted on freshly pluviated saturated and dry specimens (fly ash was gently allowed to fall in air or in a water-filled mold), remolded specimens recovered from ponds, and undisturbed specimens kept inside Shelby tubes (tube slices were carefully cut; the tube was used as the oedometer cell, and instrumented loading caps were placed on both ends). The wave velocity V_s follows a power trend with the effective vertical stress in all cases
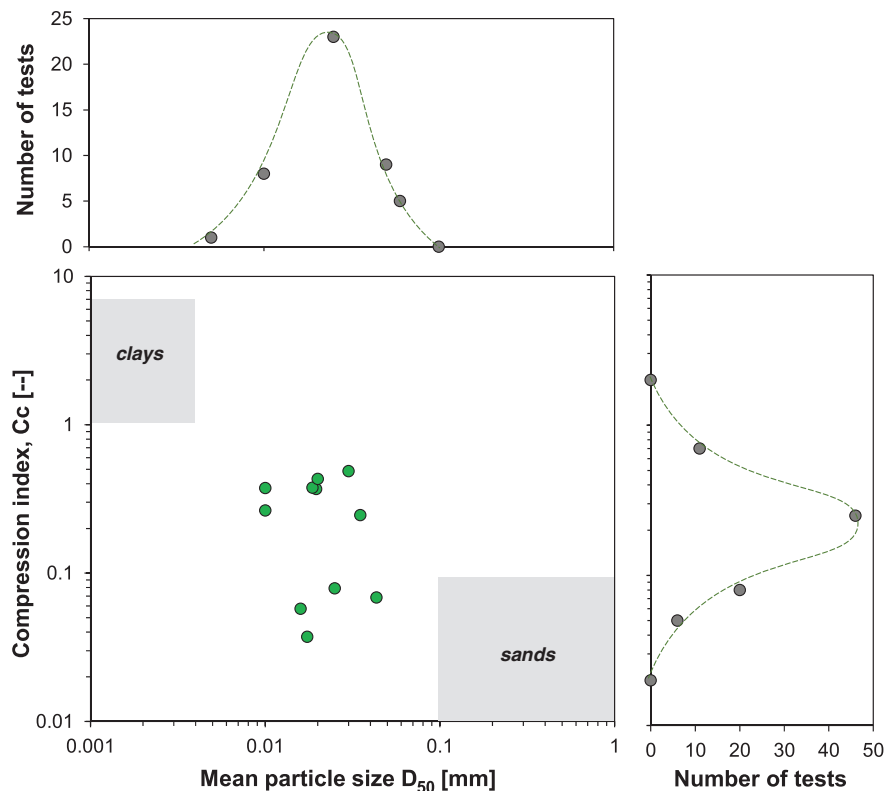
© ASCE 04019003-6 J. Geotech. Geoenviron. Eng.

J. Geotech. Geoenviron. Eng., 2019, 145(3): 04019003

Fig. 7. (Color) Compressibility and particle diameter D_{50}. The central plot shows values measured in this study (stress range of 100 kPa–1 MPa). Histograms summarize previously published fly-ash data (80 pairs). Ranges for clays and sands are shown for reference from Kulhawy and Maine (1990) and Chong and Santamarina (2016).

$$V_s = \alpha \left(\frac{\sigma'_z}{1 \text{ kPa}} \right)^{\beta} \qquad (3)$$

where factor α = shear-wave velocity (m/s) at $\sigma' = 1$ kPa; and exponent β captures the sensitivity of shear-wave velocity to changes in effective stress (Chattaraj and Sengupta 2017). Measured values for remolded and freshly prepared specimens ranged from $\alpha = 23$ to 28 m/s and $\beta = 0.29$ to 0.35; these values are in agreement with α–β trends for natural soils (Fig. 8). Fly-ash specimens that experience early diagenetic cementation exhibit higher shear-wave velocities and lower stress-sensitivity, i.e., higher α-factor and lower β-exponent (Table 2). Details will be given subsequently.

Early Diagenetic Cementation

Early diagenetic cementation may alter the evolution of densification and stiffness in fly-ash specimens. Oedometer-wetting tests and shear-wave measurements were conducted on samples recovered from different plants in southeastern United States to explore this effect.

Oedometer Tests

The effect of hydration-cementation on densification was studied using dry specimens that had not been previously exposed to water. The oedometer test procedure included an intermediate hydration stage: (1) place the dry fly ash in the oedometer cell using a combination of air pluviation and tapping to attain the targeted initial dry unit weight; (2) gradually apply vertical stress to reach $\sigma'_z = 100$ kPa; (3) while under constant σ'_z, flood the specimen from the bottom up; (4) allow the specimen to age for 120 h under
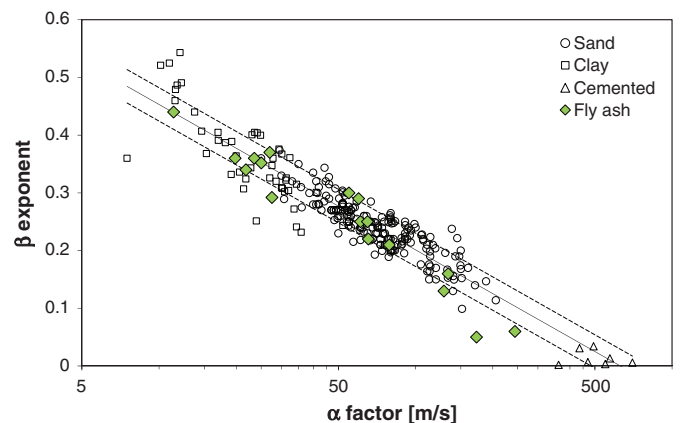

Fig. 8. (Color) Shear-wave velocity versus effective stress during loading. The α-factor and β-exponent are related as $\beta = 0.7 - 0.25 \log[\alpha/(\text{m/s})]$ for a wide range of coarse and fine-grained soils (Cha et al. 2014). Data for undisturbed and remolded fly-ash specimens fit well with the typical soil data. Low β-exponents and high α-factors indicate diagenetic cementation.

$\sigma'_z = 100$ kPa; and (5) gradually increase the vertical stress level. Fig. 9 illustrates results obtained with the same fly-ash specimen packed at two different dry unit weights. There was a minor contraction during saturation and ageing. More importantly, both specimens showed a marked change in slope, and the specimen became less compressible after wetting and ageing (observed in all specimens that experienced early diagenetic cementation) (Table 2). Fig. 9 shows that specimen compressibility decreases after wetting and aging.
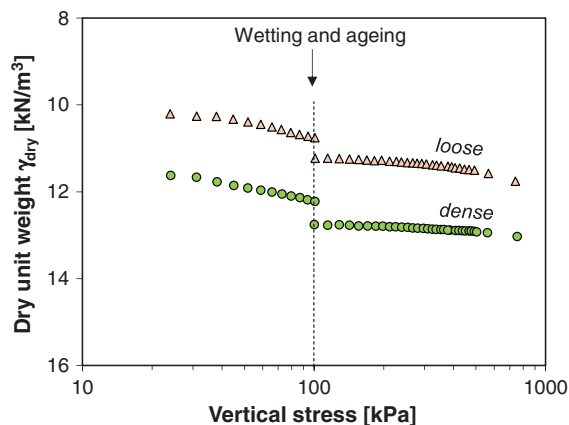
Fig. 9. (Color) Short-term diagenesis and its effects on compressibility. Test protocol: (a) dry fly ash is gradually loaded to 100 kPa in an oedometer cell; (b) water saturation and aging for 120 h takes place under constant vertical stress; and (c) loading continues.

New specimens were prepared at the end of these tests reusing the same fly ash after drying and disaggregating it to break any particle-to-particle cementation. The oedometer data do not exhibit diagenetic effects after rewetting in this case. Similarly, oedometer-wetting tests conducted on remolded specimens recovered from wet ponds (dried, disaggregated, and reconstituted) did not exhibit any significant stiffening after rewetting.

Finally, parallel oedometer tests were run on identical specimens prepared with the same fly ash used in Fig. 9, but either short or long time intervals were imposed between successive loading stages (initially dry specimens prepared by water pluviation). Slow loading tests exhibited a much stiffer response and a distinct discontinuity or sudden collapse in the load-deformation curve near the 250-kPa vertical effective stress when the newly cemented contacts break.

Small-Strain Shear-Wave Velocity
Small-strain shear-wave measurements assess the skeleton shear stiffness without altering ongoing diagenetic processes. Pastes were

prepared with fly ash that had never been wet before, specimens were formed inside Plexiglas polymethylmethacrylate cells, and caps instrumented with bender elements on both ends were added. Fig. 10(a) shows a cascade of shear-wave signatures gathered over a period of 23 days. Fig. 10(b) plots the computed shear-wave velocities; the plot includes data gathered from another fly-ash sample recovered from a wet pond after remixing. It can be seen that Specimen A-3 experiences a very pronounced increase in shear-wave velocity within the first 2 weeks following wetting. These results highlight the pronounced stiffening effect some fly-ash deposits may experience soon after wetting, particularly within the first 10 days (Table 2).

pH as Predictor of Early Diagenetic Behavior
In addition, the pH of water–fly-ash pastes (31 specimens) was measured; values ranged from a pH of 6 to 12. When compared with oedometer and shear-wave velocity data, pH emerges as a valuable diagnostic parameter: early diagenesis should be expected when pastes exhibit pH ≥ 9.5.

Summary
The aforementioned results suggest that even nonpozzolanic Class-F fly ash may experience early diagenetic cementation in relatively short time scales (hours to a week). Cementation is limited, yet specimens do become stiffer and less prone to self-weight densification. Consequently, these fly-ash deposits lock in high porosity during burial and may experience fabric collapse. The pH of fresh fly-ash pastes appears to be a valuable diagnostic tool to assess the potential for early diagenesis.

Deviatoric Load-Deformation Response

Deviatoric load tests involved 44 axial-compression triaxial tests, samples from eight different fly-ash sources, specimens prepared by either air or water pluviation (same procedure outlined previously), and both drained and undrained shear (high B-values require careful saturation procedures and backpressure, probably due to nonwetting cenospheres. Tests reported here were conducted with B-values in excess of $B \geq 0.95$). The highest effective confining stress was ≈ 200 kPa, which corresponds to a nominal pond
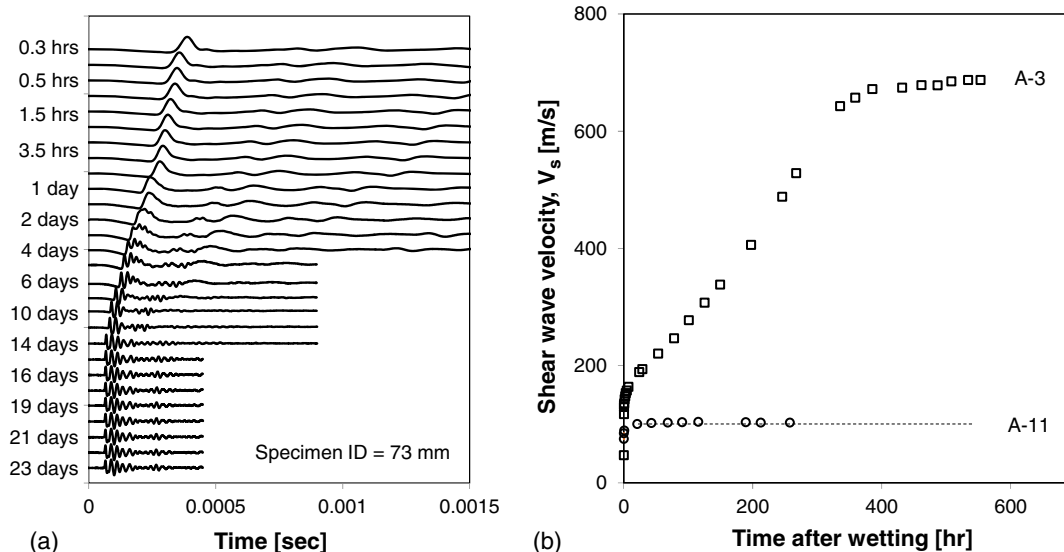

Fig. 10. Short-time diagenesis: Changes in shear-wave velocity: (a) cascade of shear-wave signatures gathered during the first 23 days after wetting; and (b) evolution of shear-wave velocity after wetting for two specimens subjected to a constant 30-kPa vertical effective stress under zero-lateral-strain boundary conditions.
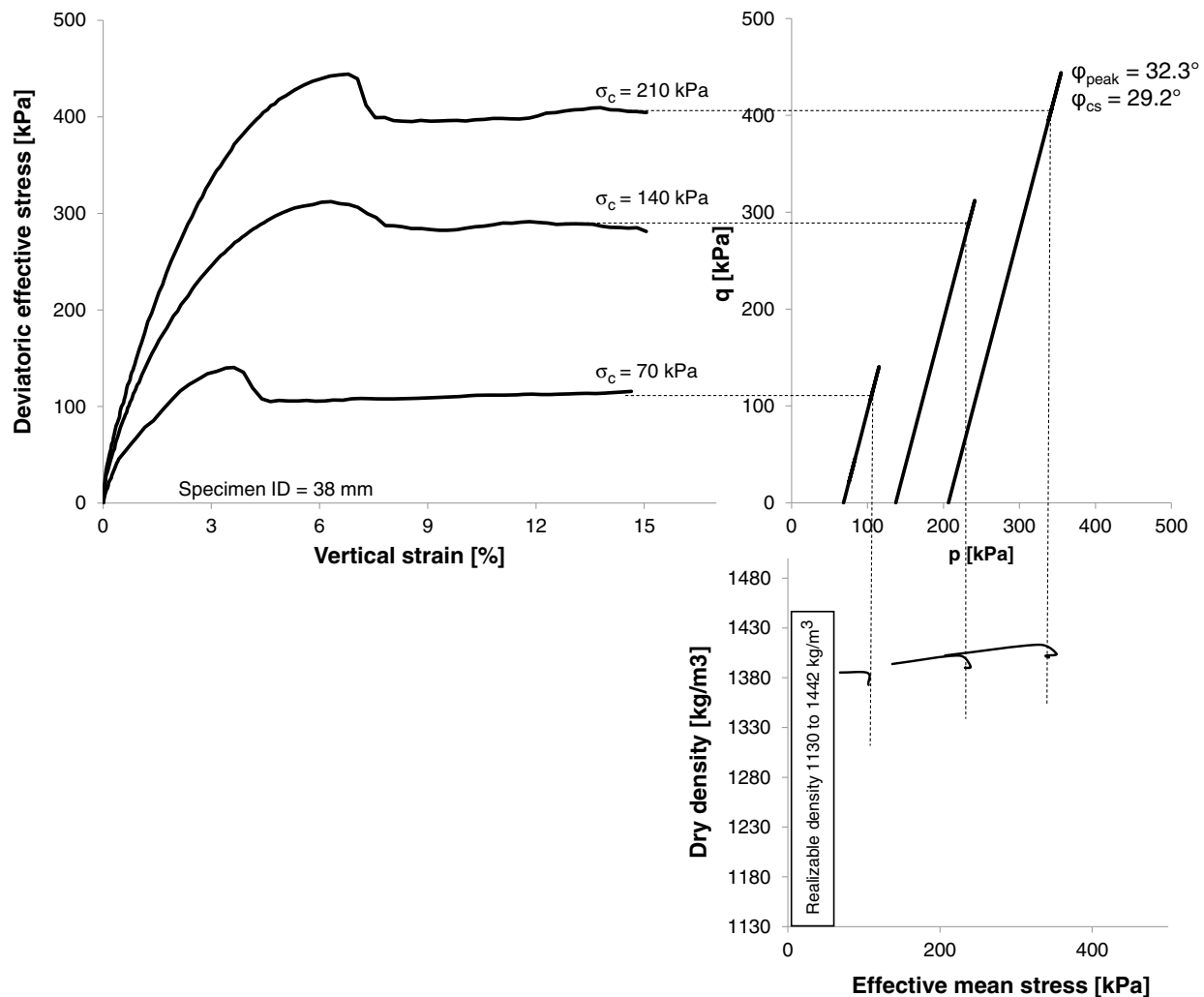
Fig. 11. Drained axial compression results for three specimens subjected to different initial isotropic effective stress levels. Data are plotted for four interconnected projections: deviatoric loading q, hydrostatic effective mean stress p', vertical strain ε_z, and dry unit weight γ_{dry}. The range of realizable unit weight for this fly ash extends beyond the scale of the plot. Deviatoric stress is defined $q = (\sigma_1' - \sigma_3')/2$, and effective mean stress is defined $p' = (\sigma_1' + \sigma_3')/2$.

depth of <25 m. Fig. 11 shows typical data for a set of three drained axial-compression (AC) triaxial tests plotted on three interconnected projections defined by shear, confinement, axial strain, and dry unit weight.

The following observations reflect these and all other test results:
- Specimens prepared with freshly remolded fly ash readily compact during isotropic loading in the absence of diagenetic cementation.
- The majority of drained test results exhibit early contraction followed by the onset of dilation at a vertical strain of $\varepsilon_z = 1$–2% and a mobilized friction angle of $\approx 25°$. Only strongly contractive sediments produce a pronounced postpeak strain softening in undrained loading.
- Most drained specimens experience visible shear localization, starting just before they reach the peak strength; dilation stops after shear localization. Undrained specimens also display shear localization.
- Peak friction angles occur after $\varepsilon_z = 5$–8% in both the drained and undrained tests.
- Constant volume friction angles vary between $\phi_{cv} = 29°$ and 36° (observed toward the end of loading as the vertical strain approaches 15%).

Fig. 12 summarizes the volume change tendencies inferred from all drained (dilation/contraction) and undrained tests (negative/positive excess pressure), versus the relative unit weights at the beginning of deviatoric loading. Tests were conducted using both freshly remolded reconstituted specimens (open markers) and undisturbed specimens trimmed from Shelby tubes (solid green circles). Four of the six contractive specimens are undisturbed specimens trimmed from Shelby tubes recovered from storage ponds. This plot suggests a transition from contractive to dilative behavior
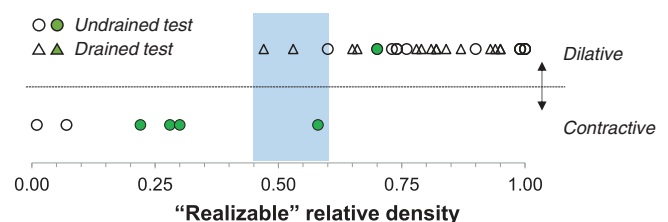

Fig. 12. (Color) Volume change tendency in drained and undrained axial compression triaxial tests versus relative density in terms of realizable unit weights.

© ASCE   04019003-9   J. Geotech. Geoenviron. Eng.

J. Geotech. Geoenviron. Eng., 2019, 145(3): 04019003

when the relative unit weight computed in terms of realizable unit weights $\gamma_{dry,min}$ and $\gamma_{dry,max}$ exceeds $D_r \approx 45–60\%$.

Conclusions

This paper documented a comprehensive study of Class-F fly ash. It included data compiled from published reports on fly ash produced around the world and results obtained from several studies conducted on fly ash produced in southeastern United States. Salient observations are as follows:

- Early diagenetic cementation hinders densification and preserves high porosity. Stability will depend on the strength of the diagenetic bonds relative to stress changes. Flow instability could take place after the failure of the containment structure if the ponded ash is saturated and in a loose contractive state.
- Chemical composition and exposure to a high boiler temperature lead to the formation of hollow cenospheres, often with accessible intraparticle porosity. This results in a wide-ranging specific gravity and affects engineering analyses related to void ratio and saturation. Therefore, correlations that are based on void ratio or porosity should be avoided.
- Instead, evaluations based on measured minimum and maximum realizable unit weights are recommended. The maximum unit weight corresponds to the conventional Proctor compaction test, whereas the minimum unit weight is obtained under gentle shear in dry conditions.
- Water pluviation tests showed significant segregation and formation of a layered structure in all fly-ash samples tested in this study. The layered deposit has anisotropic hydraulic conductivity (higher in the horizontal direction), and segregated fines accumulate to form weaker layers.
- Early diagenesis during wetting and deposition was observed in most of the dry fly-ash samples (particularly those with high pH). Diagenetic cementation prior to self-weight consolidation preserves porosity. Therefore, ponded fly ash can exhibit a collapsible structure with pronounced contractive tendencies.
- In the absence of early diagenetic cementation, experimental results show that wet disposal gives rise to dilative ponded ash in the upper 20–25 m when subjected to monotonic shear loading. On the other hand, flow instability could take place—after the failure of the containment structure—if the ponded ash is saturated and early diagenetic cementation hindered densification.

Acknowledgments

References

ACAA (American Coal Ash Association). 2014. "2014 coal combustion product production and use survey report." Accessed March 15, 2016. https://www.acaa-usa.org/Portals/9/Files/PDFs/2014ReportFinal.pdf.

Acosta, A. H., T. Edil, and C. Benson. 2003. *Soil stabilization and drying using fly ash*. Geo Engineering Rep. Madison, WI: Univ. of Wisconsin-Madison.

Aineto, M., A. Acosta, J. M. Rincon, and M. Romero. 2005. "Production of lightweight aggregates from coal gasification fly ash and slag." In *Proc., World of Coal Ash Conf.*, 11–15. Lexington, KY.

Aineto, M., A. Acosta, J. M. Rincón, and M. Romero. 2006. "Thermal expansion of slag and fly ash from coal gasification in IGCC power plant." *Fuel* 85 (16): 2352–2358. https://doi.org/10.1016/j.fuel.2006.05.015.

Amonette, J., J. Kim, C. Russell, A. Palumbo, and W. Daniels. 2003. "Enhancement of soil carbon sequestration by amendment with fly ash." In *Proc., World of Coal Ash Conf.* Lexington, KY.

ASTM. 2007a. *Standard practice for dry preparation of soil samples for particle-size analysis and determination of soil constants*. ASTM D421-85. West Conshohocken, PA: ASTM.

ASTM. 2007b. *Standard test method for particle-size analysis of soils*. ASTM D422-63. West Conshohocken, PA: ASTM.

ASTM. 2009. *Standard test method for density of hydraulic cement*. ASTM C188. West Conshohocken, PA: ASTM.

ASTM. 2017a. *Standard test methods for liquid limit, plastic limit, and plasticity index of soils*. ASTM D4318. West Conshohocken, PA: ASTM.

ASTM. 2017b. *Standard test methods for sampling and testing fly ash or natural pozzolans for use in portland-cement concrete*. ASTM C311/311M. West Conshohocken, PA: ASTM.

Bin-Shafique, M. S., C. H. Benson, and T. B. Edil. 2002. *Leaching of heavy metals from fly ash stabilized soils used in highway pavements*. Madison, WI: Dept. of Civil and Environmental Engineering, Univ. of Wisconsin-Madison.

BS (British Standards). 1990. *Soils for civil engineering purposes. Part 2: Classification tests*. BS 1377-2. London: BS.

Cha, M., J. C. Santamarina, H. S. Kim, and G. C. Cho. 2014. "Small-strain stiffness, shear wave velocity and soil compressibility." *J. Geotech. Geoenviron. Eng.* 140 (10): 06014011. https://doi.org/10.1061/(ASCE)GT.1943-5606.0001157.

Chattaraj, R., and A. Sengupta. 2017. "Dynamic properties of fly ash." *J. Mater. Civ. Eng.* 29 (1): 04016190. https://doi.org/10.1061/(ASCE)MT.1943-5533.0001712.

Cheerarot, R., and C. Jaturapitakkul. 2004. "A study of disposed fly ash from landfill to replace portland cement." *Waste Manage.* 24 (7): 701–709. https://doi.org/10.1016/j.wasman.2004.02.003.

Chong, S. H., and J. C. Santamarina. 2016. "Soil compressibility models for wide stress range." *J. Geotech. Geoenviron. Eng.* 142 (6): 06016003. https://doi.org/10.1061/(ASCE)GT.1943-5606.0001482.

Cousens, T. W., and D. I. Stewart. 2003. "Behaviour of a trial embankment on hydraulically placed PFA." *Eng. Geol.* 70 (3–4): 293–303. https://doi.org/10.1016/S0013-7952(03)00097-8.

Das, S. K., and Y. Yudhbir. 2006. "Geotechnical properties of low calcium and high calcium fly ash." *Geotech. Geol. Eng.* 24 (2): 249–263. https://doi.org/10.1007/s10706-004-5722-y.

DiGioia, A. M., Jr., G. F. Brendel, D. J. Spaeder, N. J. Balsamo, and L. C. Shumway. 1995. *Coal ash disposal manual*. 3rd ed. Palo Alto, CA: Electric Power Research Institute.

Du, L., E. Lukefahr, and A. Naranjo. 2013. "Texas Department of Transportation fly ash database and the development of chemical composition-based fly ash alkali-silica reaction durability index." *J. Mater. Civ. Eng.* 25 (1): 70–77. https://doi.org/10.1061/(ASCE)MT.1943-5533.0000564.

Fenelonov, V. B., M. S. Mel'gunov, and V. N. Parmon. 2010. "The properties of cenospheres and the mechanism of their formation during high-temperature coal combustion at thermal power plans." *KONA Powder Part. J.* 28: 189–208. https://doi.org/10.14356/kona.2010017.

Fisher, G. L., D. P. Y. Chang, and M. Brummer. 1976. "Fly ash collected from electrostatic precipitators: Microcrystalline structures and the mystery of the spheres." *Science* 192 (4239): 553–555. https://doi.org/10.1126/science.192.4239.553.

Fisher, G. L., and D. F. S. Natusch. 1979. "Size dependence of the physical and chemical properties of coal fly ash." *Anal. Methods Coal Coal Prod.* 3: 489–541. https://doi.org/10.1016/B978-0-12-399903-0.50023-4.

Gray, D. H., and Y.-K. Lin. 1972. "Engineering properties of compacted fly ash." *J. Soil Mech. Found. Div.* 98 (SM4): 361–380.

Jang, J., and J. C. Santamarina. 2016. "Fines classification based on sensitivity to pore-fluid chemistry." *J. Geotech. Geoenviron. Eng.* 142 (4): 06015018. https://doi.org/10.1061/(ASCE)GT.1943-5606.0001420.

Jang, J., and J. C. Santamarina. 2017. "Closure to "Fines classification based on sensitivity to pore-fluid chemistry" by Junbong Jang and

© ASCE 04019003-10 J. Geotech. Geoenviron. Eng.

J. Geotech. Geoenviron. Eng., 2019, 145(3): 04019003

J. Carlos Santamarina." *J. Geotech. Geoenviron. Eng.* 143 (7): 07017013. https://doi.org/10.1061/(ASCE)GT.1943-5606.0001694.

Kaniraj, S. R., and V. Gayathri. 2004. "Permeability and consolidation characteristics of compacted fly ash." *J. Energy Eng.* 130 (1): 18–43. https://doi.org/10.1061/(ASCE)0733-9402(2004)130:1(18).

Kim, B., and M. Prezzi. 2008. "Evaluation of the mechanical properties of class-F fly ash." *Waste Manage.* 28 (3): 649–659. https://doi.org/10.1016/j.wasman.2007.04.006.

Kim, B., M. Prezzi, and R. Salgado. 2005. "Geotechnical properties of fly and bottom ash mixtures for use in highway embankments." *J. Geotech. Geoenviron. Eng.* 131 (7): 914–924. https://doi.org/10.1061/(ASCE)1090-0241(2005)131:7(914).

Kulhawy, F. H., and P. W. M. Maine. 1990. *Manual on estimating soil properties for foundation design*. Rep. No. EPRI-EL-6800. Palo Alto, CA: Electric Power Research Institute.

Lin, S. Y., M. Hirato, and M. Horio. 1994. "The characteristics of coal char gasification at around ash melting temperature." *Energy Fuels* 8 (3): 598–606. https://doi.org/10.1021/ef00045a01410.1021/ef00045a014.

Mishra, D. P., and S. K. Das. 2008. "Consolidation characteristics of stowed pond ash and pond ash-lime mixture." *J. Inst. Eng.* 89: 9–18.

Mishra, M. K., and U. M. R. Karanam. 2006. "Geotechnical characterization of fly ash composites for backfilling mine voids." *Geotech. Geol. Eng.* 24 (6): 1749–1765. https://doi.org/10.1007/s10706-006-6805-8.

Palmer, B. G., T. B. Edil, and C. H. Benson. 2000. "Liners for waste containment constructed with class F and C fly ashes." *J. Hazard. Mater.* 76 (2–3): 193–216. https://doi.org/10.1016/S0304-3894(00)00199-0.

Pandian, N. S. 2004. "Fly ash characterization with reference to geotechnical applications." *J. Ind. Inst. Sci.* 84 (6): 189–216.

Park, J., and J. C. Santamarina. 2017. "Revised soil classification system for coarse-fine mixtures." *J. Geotech. Geoenviron. Eng.* 143 (8): 04017039. https://doi.org/10.1061/(ASCE)GT.1943-5606.0001705.

Prashanth, J. P., P. V. Sivapullaiah, and A. Sridharan. 2001. "Pozzolanic fly ash as a hydraulic barrier in landfills." *Eng. Geol.* 60 (1–4): 245–252. https://doi.org/10.1016/S0013-7952(00)00105-8.

Premchitt, J., and N. C. Evans. 1995. *The use of PFA in reclamation*. Geo Rep. No. 24. Wan Chai, Hong Kong: Civil Engineering Dept., Hong Kong Government.

Ren, X. W., and J. C. Santamarina. 2018. "The hydraulic conductivity of sediments: A pore size perspective." *Eng. Geol.* 233: 48–54. https://doi.org/10.1016/j.enggeo.2017.11.022.

Reyes, A., and M. Pando. 2007. "Evaluation of CFBC fly ash for improvement of soft clays." In *Proc., World of Coal Ash Conf.* Covington, KY.

Senol, A., M. S. Bin-Shafique, T. B. Edil, and C. H. Benson. 2003. "Use of class C fly ash for stabilization of soft subgrade." In *Proc., 5th Int. Congress on Advances in Civil Engineering*. Istanbul, Turkey: Istanbul Technical Univ.

Siddique, R., W. Prince, and S. Kamali. 2007. "Influence of utilization of high-volumes of class F fly ash on the abrasion resistance of concrete." *Leonardo Electron. J. Pract. Technol.* 10: 13–28.

Song, W., Y. Dong, Y. Wu, and Z. Zhu. 2011. "Prediction of temperature of critical viscosity of coal ash slag." *Am. Inst. Chem. Eng. J.* 57 (10): 2921–2925. https://doi.org/10.1002/aic.12500.

Torrey, S. 1978. *Coal ash utilization: Fly ash, bottom and slag*. Park Ridge, IL: Noyes Data Corporation.

Trivedi, A., and V. K. Sud. 2004. "Collapse behavior of coal ash." *J. Geotech. Geoenviron. Eng.* 130 (4): 403–415. https://doi.org/10.1061/(ASCE)1090-0241(2004)130:4(403).

Trivedi, A., and V. K. Sud. 2007. "Settlement of compacted ash fills." *Geotech. Geol. Eng.* 25 (2): 163–176. https://doi.org/10.1007/s10706-006-9101-8.

Tu, W., B. Zand, M. A. Ajlouni, T. S. Butalia, and W. E. Wolfe. 2007. "The consolidation characteristics of impounded class F fly ash: A case history." In *Proc., World of Coal Ash Conf.* Covington, KY.

Young, S. C. 1993. *Physical and hydraulic properties of fly ash and other by-products from coal combustion*. EPRI Rep. Palo Alto, CA: Electric Power Research Institute.

© ASCE   04019003-11   J. Geotech. Geoenviron. Eng.

J. Geotech. Geoenviron. Eng., 2019, 145(3): 04019003